Structural, magnetic and GMR properties of FeCo(Cu)/Cu magnetic multilayers electrodeposited at high cathode potentials of the magnetic layer

A. TEKGÜL[a,*], T. ŞAHIN[b], H. KÖÇKAR[b], M. ALPER[a]
[a]*Uludag University, Physics Department, Science and Literature Faculty, TR-16059, Bursa, Turkey*
[b]*Balıkesir University, Physics Department, Science and Literature Faculty, TR-10145, Balıkesir, Turkey*

Structural, magnetic and giant magnetoresistance properties of the electrochemically deposited FeCo(Cu)/Cu multilayers at the various cathode potentials for magnetic layers were investigated. The cathode potentials were –1.8, –2.0, –2.5 and –2.8 V for magnetic layers and –0.3 V for non-magnetic layers with respect to a saturated calomel electrode. The multilayers have a face-centred-cubic structure. The obtained composition was found to be close the nominal composition at –2.8 V cathode potential. The highest giant magnetoresistance value (16.50 %) was obtained in the multilayer produced at –1.8 V. The highest sensitivity was found in the multilayer produced at –1.8 and –2.8 V.

(Received April 16, 2019; accepted April 9, 2020)

Keywords: Electrochemical deposition, High giant magnetoresistance, High cathode potential, Iron cobalt copper multilayer

1. Introduction

The electrochemical deposition is one of the technique to produce the nano-technological devices [1-3]. The primary mechanism of these devices is the giant magnetoresistance (GMR) effect [4-6]. The GMR generally is observed in the multilayer systems, which consist of two, ferromagnetic layers separated a non-magnetic layer. Between the magnetic and non-magnetic intermediate surface, the scattering is caused the significant changes in its resistance. Therefore, the roughness of the intermediate surface provides the high resistance in the multilayer [7-9]. And also, the antiferromagnetic coupling between the adjacent magnetic layer plays a major role and the magnetic moments in the sub-layers can change their directions when the external magnetic field is applied.

The GMR effect has been observed by Peter Grünberg [7] and Albert Fert [8] in Fe/Cr/Fe multilayered nanostructure which is grown by the molecular beam epitaxy. The molecular beam epitaxy is a popular technique to produce magnetic multilayers but, the producing cost and the requirement of the high vacuum are the disadvantages of it. In 1993, Alper et al. have observed the GMR effect in Cu/CoNiCu superlattice produced by the electrochemical deposition technique [9]. The electrochemical deposition is an alternative of the techniques needed the high vacuum. The main advantages of this technique are the cheapness, the easy production without a vacuum and the produce of the desired geometry. Such Co/Cu [10-17], FeCo/Cu [18-22] multilayered systems have been produced by the electrochemical technique. Generally, the single or the dual baths are used to produce these multilayered systems. The single bath is more preferred than the dual bath because of the contamination and the oxidation risk of the dual bath technique. Therefore, the applied cathode potentials play an important role in the single bath. And also in the single bath, the noble elements electrochemically deposit on the cathode in both low and high potentials and hence, their concentration in the electrolyte must be controlled. In the producing the FeCo/Cu multilayer from the single bath, the low current pulse (low cathode potential) provides the deposition of the Cu atoms, and the high current pulse (high cathode potential) causes the deposition of the Co and the Fe atoms. But, the Cu is a noble element and a few percent of its deposits together with the Co and the Fe atoms in the magnetic layers. Also, when the dissolution of Co and Fe can occur during the Cu deposition pulse [9] and hence, the Cu elements can be deposited.

Electrochemical deposited Co(Cu)/Cu multilayers have been mostly studied and these exhibits the high GMR values [14, 15, 23-31]. The magnetic layers have a strong uniaxial magnetocrystalline anisotropy due to the Co atoms. With the separation of the Cu layer, the magnetic interaction of the adjacent magnetic layers decreases in these multilayers. The Cu atoms in the magnetic sublayers provide to reduce the magnetic hardening of the multilayer [32]. The FeCo alloy studies show that the alloy exhibits the soft magnetic property because of the weak magnetocrystalline anisotropy and magnetostriction of the Fe atoms [33]. Similarly, when the Fe is added the Co(Cu)/Cu multilayered system, the FeCo(Cu)/Cu multilayer presents both the high GMR value and the more sensitive GMR curve than the Co(Cu)/Cu multilayer [34]. Moreover, the Fe causes to reduce the magnetic hardness and hence, the multilayer has the low coercivity [20]. For

all that, the electrochemical deposition of the multilayer with Fe content is hard from the electrolyte. Fe is the sensitive against the water and oxygen. Thereupon, the oxidation of Fe ions can occur in the electrolyte and hence, the concentration of the Fe ions decreases. Consequently, the electrolyte can be used a short time [20].

Such FeCo(Cu)/Cu multilayers with the high GMR have been used in the many industrial applications as the read head in the disk drive, the sensitive detection of magnetic fields in magnetometers [1-3]. In this aspect, the FeCo(Cu)/Cu magnetic multilayers have a potential for the new detection applications. Despite producing difficulty of the FeCo(Cu)/Cu multilayer, the several studies [20-22, 35-41] have been reported by the electrochemical deposition technique. However, the cathode potential for the magnetic layers is applied to below −1.8 V versus the saturated calomel electrode (SCE). In the present study, we investigated the electrochemical deposited FeCo(Cu)/Cu multilayers produced at over −1.8 V versus SCE. The electrochemical, structural, magnetic and high GMR properties of these multilayers were presented.

2. Experimental

The FeCo(Cu)/Cu multilayers were produced on Ti substrates by electrochemical deposition. In the produce, two-pulse plating from a single-bath was applied on a substrate. The electrolyte was prepared with $CoSO_4$ $7H_2O$, $FeSO_4$ $7H_2O$, and $CuSO_4$ $4H_2O$. The additive substance, H_3BO_3 was used to regulate the electrolyte. The concentration of the Fe, Co, and Cu were determined by the inductively coupled plasma-mass spectrometer and the 0.470 M Co, 0.100 M Fe and 0.030 M Cu were found in the electrolyte. The pH value of freshly prepared electrolytes was 2.5 ± 0.2. The multilayers were deposited in a cell with three electrodes using a potentiostat/galvanostat controlled by a personal computer. The deposition potentials were determined from the cyclic voltammogram of the electrolyte. The non-magnetic layers were deposited at a −0.3 V versus SCE and the cathode potential for the magnetic layers was changed from −1.8 to −2.8 V versus SCE. The bilayer numbers were chosen so that the nominal thickness is about 3 μm in the area of ~2.9 cm^2 and the layer thickness was held constant at 6 nm. Upon completion of growth, the films were peeled off their substrates mechanically. The charge flowing through the system was recorded during the potentiostatic pulse. Then, the nominal thickness can be calculated from Faraday's law using Eq. 1.

$$d = \frac{Q\eta}{zFA}\frac{M}{\rho} \tag{1}$$

Here, the Q, z, F and A are the quantity of deposited metals, valance electrons of its metal ion, Faraday constant and surface area, respectively. M is the molar weight, and ρ is the density of its metal ion. Here, the vital parameter is the current efficiency, η which for the Co-rich layer deposition was calculated by assuming that the Cu layer deposition took place at 100% current efficiency [42].

The morphological and elemental analyzes were performed by the scanning electron microscopy (SEM) with the energy dispersive X-ray spectrometry (EDX). The X-ray diffraction (XRD) technique was used to the structural analyze of the multilayers with the help of a Philips Analytical XRD (PW 3040/60 model) with Cu-K_α radiation in the range of 2θ=30-80°. The XRD spectra were refined with the Rietveld refinement method by using the FullProf software.

The magnetic properties were measured with the vibrating sample magnetometer (VSM, ADE technologies DMS-EV9 Model) in the range of ±2 T magnetic field. The measurements were realized as to be parallel and perpendicular to the magnetic field. And also, MR measurements were carried out in magnetic fields in the range of ±1.2 T at room temperature with the Van der Pauw (VDP) technique by using the Eq. 2.

$$R(\%) = \frac{R(H) - R_{\min}}{R_{\min}} \times 100 \tag{2}$$

In this relation, $R(H)$ is the measured electrical resistance value at any magnetic field, and $R_{\min}$ is the minimum measured resistance. The magnetic field was applied both parallel and perpendicular to the current flowing in the film plane to measure the longitudinal (LMR) and transverse magnetoresistances (TMR), respectively.

3. Results and discussion

Fig. 1 shows the current-time transients of the FeCo(Cu)/Cu multilayer produced with −1.8 V cathode potential during growth for the first few layers. In the figure, the dotted and dashed lines indicate the magnetic and non-magnetic layer deposition, and the dotted-dashed line shows the capacitive transient. As seen in the figure, the two anodic pulses occur to form a bi-layer. The low anodic pulse of them relates the Cu layer deposition and the high one belongs the FeCoCu layer deposition. In the single bath, the noble Cu can reduce more easily than the less noble Fe and Co. On the other hand, the anomalous co-deposition may occur in the electrochemical deposition [30, 43] and hence, the less noble elements can be abnormally reduced [44]. In our study, relatively lower cathode potentials (below -3.0 V) prevent the Co ions during the electrochemical deposition. Since the Co atoms prefer the face-centred cubic formation at higher cathode potential (-3.0 V and above). The Co atoms choose the hexagonal-close-package in lower potentials [45]. Consequently, the Fe ions abnormally reduce on the substrate and the Co amount decreases in the layers. On the other hand, there is not enough Fe ion deposition because of low molarity of the Fe in the electrolyte and therefore, the Cu deposits with Fe and Co in the magnetic

layer. The cathodic pulse is a capacitive transient, and after negative pulses of the FeCoCu and Cu layer deposit. The capacitive transient causes a high potential in the cathode and this high potential dissolves the last deposited layer. The nominal thickness can be calculated from the current transient curves by using Eq. 1. The calculated percentages of the FeCo and Cu are given in Table 1.

The surface morphology of the FeCo(Cu)/Cu multilayers produced at the various cathode potentials was performed by the SEM. The SEM images of the multilayers are given in Fig. 2.a-d. The images of all multilayers were taken by applying 15 kV accelerating voltage. The distribution of the particles form in the surface of the multilayer at −1.8 and −2.0 V cathode potential in Fig 2.a and b is grainier than that of higher potentials. At −2.5 V cathode potential, the particles form a uniform surface, and also, some particles occur on this uniform surface in Fig. 2.c. In Fig. 2.d, the surface of the multilayer has smaller particles than that of multilayers produced at –1.8, –2.0 and –2.5 V. Additionally, there are some particles on the surface as similar as Fig. 2.c.

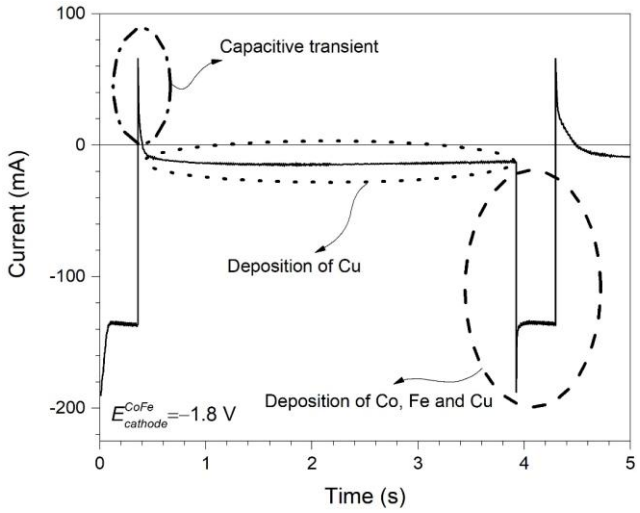

Fig. 1. Current-time transients of the FeCoCu/Cu multilayer produced with –1.8 V (SCE) cathode potential

The elemental analysis was performed by EDX and the obtained results are given in Table 1. The Cu deposition increases with increasing the cathode potential. The Fe and the Co atoms more deposit at the high cathode potentials. As seen Table 1, the compositions calculated with Eq.1 are quite compatible with the EDX results. According to these results, the expected composition of the multilayer occurs at −2.8 V cathode potential. At the low cathode potentials, the thickness of magnetic layers is the lower than the nominal thickness.

Fig. 3.a and b show the refined XRD pattern of FeCoCu/Cu which produced at −1.8 and −2.5 V cathode potential, respectively. In the figure, the grey circles and thick black lines show the observed and calculated patterns. The difference between observed and calculated patterns is indicated by the thin black line. The Bragg positions are presented in the lower part. In Fig. 3.a, the peaks are observed at $2\theta \approx 44°$, 51°, 74°, 91° and 97°. These are related with (111), (200), (220), (311) and (222) planes of the face centred cubic (fcc) structure (space group: *Fm-3m*). As seen the Co and Cu Bragg positions, the multilayers adopt the cubic structure with both magnetic and non-magnetic layers. However, the peak at $2\theta \approx 44°$ begins to rise in the multilayer produced at –2.5 V cathode potential in Fig. 3.b. This peak is related to (110) of the body centred cubic Fe (space group *Im-3m*).

Table 1. The composition of the FeCo(Cu)/Cu multilayer with EDX and calculated by Eq. 1

Cat. Pot. (V)	The composition of FeCoCu/Cu multilayer with EDX			The composition of FeCoCu/Cu multilayer calculated by Eq.1.	
	Co at.%	Fe at.%	Cu at.%	FeCo at.%	Cu at.%
–1.8	20.89	10.00	69.12	34.30	65.70
–2.0	12.85	6.67	80.48	23.93	76.07
–2.5	26.06	14.30	59.64	38.50	61.50
–2.8	28.17	15.48	56.34	40.48	59.52

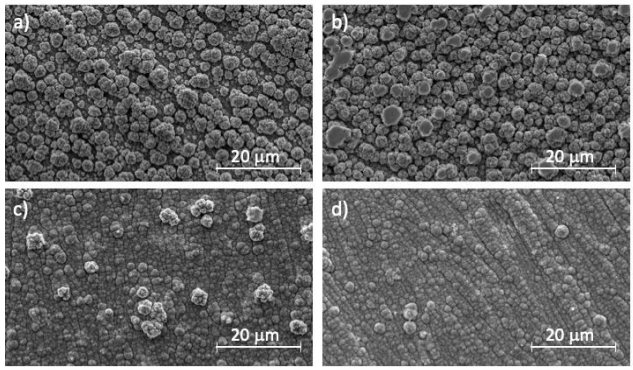

Fig. 2. The SEM images of the multilayers produced with the cathode potential of a) –1.8 V, b) –2.0 V, c) –2.5 V and d) –2.8 V. The images are the same magnification (4000X)

As observed in EDX results, the deposition of the Fe increases with the increasing cathode potential and the amount of the Fe is higher at −2.5 and −2.8 V than other cathode potentials. Therefore, the (110) peaks begin the shift through the high 2θ value. The calculated crystallite sizes are 40, 60, 72 45 and 43 nm as the cathode potentials increase from −1.6 to −2.8 V, respectively. The calculated lattice parameters are 0.3607, 0.3598, 0.3597 and 0.3580 nm. These values are between the lattice parameters of bulk Cu (0.361 nm) and Co (0.358 nm), and the Co amount increases in the composition as the cathode potential increases. When these lattice parameters are compared with the similar studies in the literature, the calculated lattice parameters are close to the values at Refs. [22, 36, 38-41].

The magnetic property of the multilayers was determined with the hysteresis curves and that of the multilayer produced at −2.8 V cathode potential is presented in Fig. 4. The field was applied both parallel (black line) and perpendicular (grey dash-dot line) to the film plane to measure. As seen from the figure, the easy axis of the multilayer is the parallel and the similar behaviour has been observed in Ref. [46]. The saturation magnetization, M_S, was found to be 164.26, 122.57, 56.35 and 47.50 Am^2/kg with increasing cathode potential in the parallel configuration. In this case, the Cu amount at −1.8 and −2.0 V is more than the multilayer produced at −2.5 and −2.8 V cathode potential. Therefore, the decreasing Cu layer thickness due to the cathode potential causes the increasing in the exchange interaction between the magnetic moment of the FeCo layers. The magnetic layers could prefer the antiferromagnetic orientation and hence, the magnetization decreases due to the cathode potential. For the parallel configuration of the multilayers produced at –1.8 V, –2.0 V, –2.5 V and –2.8 V, the obtained coercivity values (H_C) are 4, 3, 5 and 6 mT, respectively. And also, the H_C values for perpendicular configuration of these multilayers are found to be 13, 14, 15 and 22 mT.

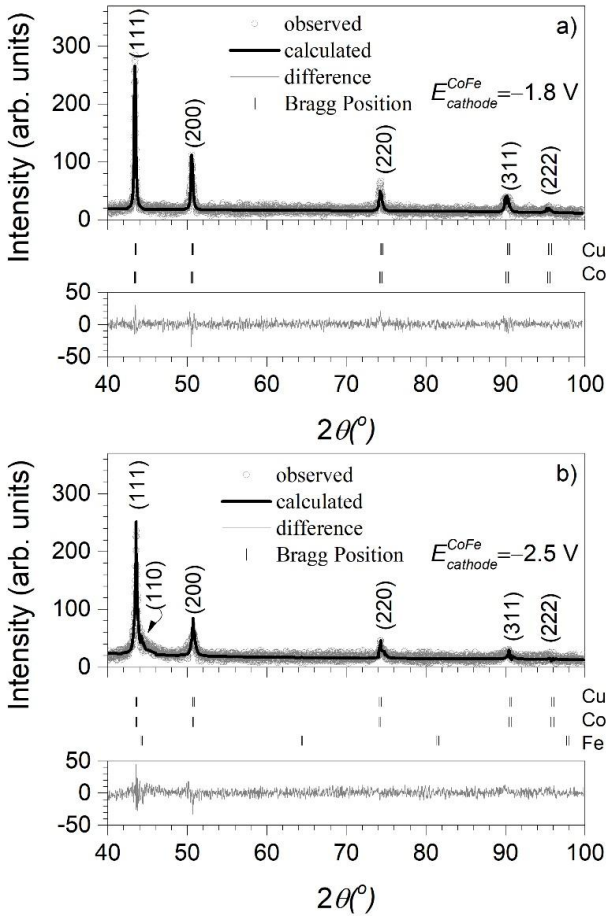

Fig. 3. Refined XRD pattern of FeCo(Cu)/Cu produced at (a) –1.8 V and (b) –2.5 V in the range of 40-100°. Grey circle is the observed pattern, the thick black line is the calculated pattern and the difference of these is showed black line patterns at the bottom in each figure. Bragg positions of all structures are indicated

The preferred orientation of the multilayer causes the different H_C and the increasing of the Co in the layers causes the rise of the H_C due to the cathode potential as seen in the EDX. Here, the Co has a higher crystal anisotropy than that of the Fe [47] and therefore, the coercivity of the multilayers increases with Co content. Although, the low H_C observed in the −2.0 V cathode potential and this may be due to the grainy surface of the multilayer. The obtained values are given in Table 2.

The MR measurements were performed with the VDP method at room temperature, and the results are given in Fig. 5.a-d. The GMR behaviour was observed in both LMR and TMR in all multilayer. The values of the MR % are given in Table 2. The high GMR was found in the multilayer produced at −1.8 V cathode potential. The anisotropic magnetoresistance (AMR) of the multilayers was calculated with AMR=|LMR−TMR| in Table 2. The AMR is due to the relatively large Co layer thickness [42] and the obtained AMR values except the multilayer produced at −2.8 V cathode potential are compatible with the EDX results. In the multilayer produced at –2.8 V, the Fe amount is higher than the other multilayers and hence, the AMR may be decreased with high amount soft magnetic Fe. Moreover, the coercivity values of the multilayer at −1.8 and −2.5 V are higher and therefore, a splitting occurs in both LMR and TMR measurements.

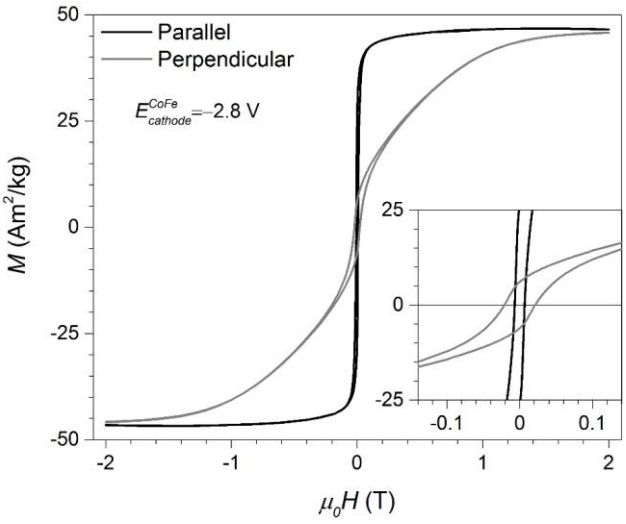

Fig. 4. The hysteresis curve of the multilayer produced at –2.8 V cathode potential. Black and grey dash-dot lines indicate the parallel and perpendicular measurements to the plane

The GMR field sensitivities (S) were defined by (3),

$$S = \frac{GMR}{HS50} \tag{3}$$

where GMR is the maximum MR value of the multilayer and HS50 is the field change to reduce the 50 % of the GMR value [48] and the calculated sensitivities are given

in Table 2. The results revealed that the multilayers produced at −1.8 and −2.8 V cathode potential have high GMR sensitivity.

Table 2. The magnetization and magnetoresistance properties of the FeCo(Cu)/Cu multilayers

FeCoCu/Cu	−1.8 V	−2.0 V	−2.5V	−2.8V
M_S (Am^2/kg) Parallel	164.26	122.57	56.35	47.50
H_C (mT) Parallel	3.98	2.78	5.18	6.45
H_C (mT) Perpendicular	13.34	13.93	14.82	21.51
LMR (%)	12.38	7.40	5.76	8.04
TMR (%)	16.50	8.02	10.68	5.97
AMR (%)	4.12	0.62	4.92	2.07
GMR sensitivity (%/mT) in LMR	0.49	0.10	0.34	0.44
GMR sensitivity (%/mT) in TMR	0.55	0.09	0.36	0.38

When the obtained MR results compare the similar multilayers (see Table 4 in Ref. 41), the electrochemical deposited FeCo(Cu) (6 nm)/Cu (6 nm) multilayers have been investigated in Refs. 21, 38 and 40. The cathode potential for the magnetic layer has been used –1.5 V for Refs. 38, 40 (the electrolyte contains 0.05 M Fe) and –1.6 V for Ref. 21 (the electrolyte contains 0.1 M Fe). The MR results in Refs. 38 and 40 are higher than that of the present study. On the other hand, the MR change is 12 % in the Ref. 21 and this value has been obtained at 2.7 pH. The 16.50 % MR change was obtained for -1.8 V cathode potential in the present study and the GMR sensitivity for high cathode potentials is higher than the Refs. 21, 38 and 40. This sensitivity is due to higher Fe content in the multilayers. Consequently, high GMR values has been obtained at –1.5 V for the magnetic layer but, high GMR sensitivity can be obtained at high cathode potential values.

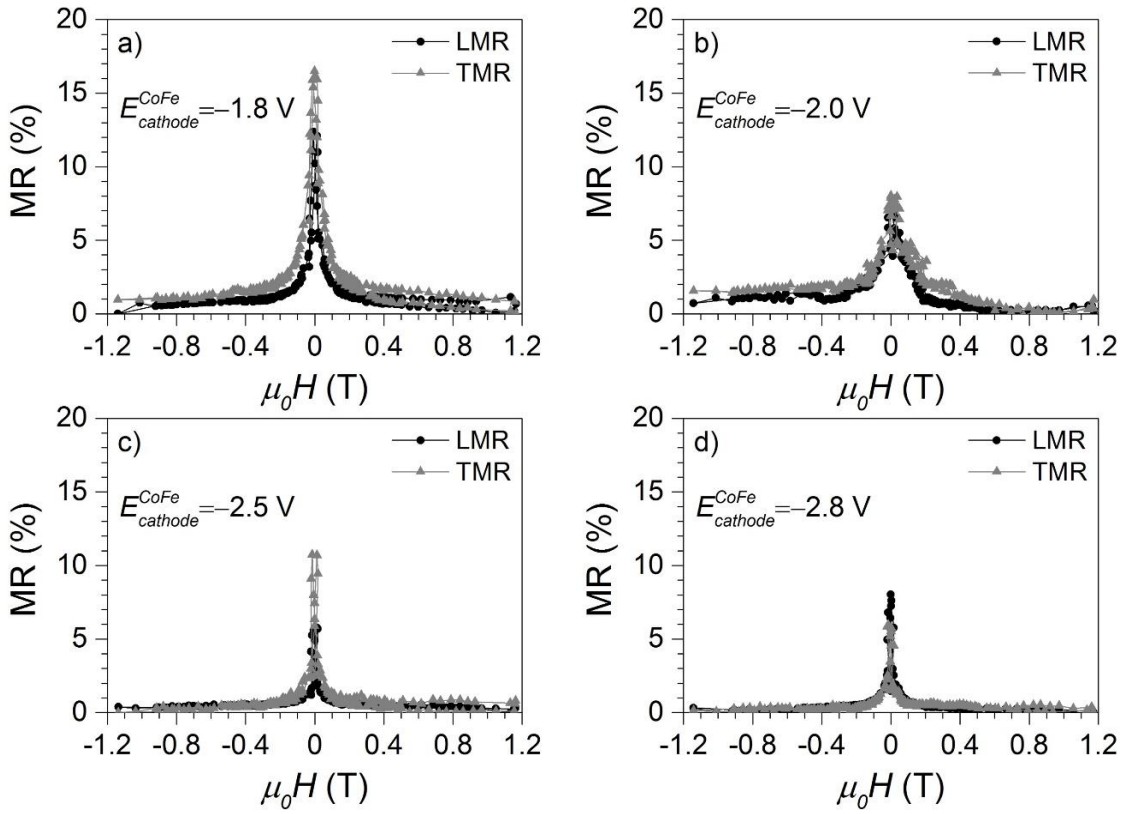

Fig. 5. Magnetoresistance measurements of the multilayers produced at a) –1.8 V b) –2.0 V c) –2.5 V and d) –2.8 V

4. Conclusions

In present study, FeCo(Cu)/Cu multilayers were produced at various high cathode potentials for the magnetic layers from the electrolyte containing 0.470 M Co, 0.100 M Fe, 0.030 M Cu and 0.5 M H_3BO_3 by the electrochemical deposition technique. The pH level of the electrolyte was freshly checked and kept constant at 2.5 ±

0.2. The surface morphology of the multilayers was investigated by the SEM. The surface of multilayers at -1.8 V and -2.0 V was found in irregular form. The compositions were determined by the EDX component of the SEM and the nominal compositions were calculated from the current-time curves, and the results are quite compatible with the EDX results. The EDX results indicate that the deposition amounts of Co and Fe increase with increasing the cathode potential. The structural characterizations were performed by the XRD technique and the patterns were refined using Rietveld refinement by the FullProf software. The crystal structure of the multilayers is face-centred-cubic (space group *Fm-3m*). The Bragg positions related to Co and Cu indicate that the crystal structure of the multilayers adopt the cubic crystal structure. However, the peak at $2\theta \approx 44°$ of the body-centred-cubic (bcc) Fe (space group *Im-3m*) begins to rise in the multilayer produced at −2.5 and −2.8 V cathode potential because of the high amount of the Fe (bcc) in the magnetic layers. The magnetic properties were determined by the VSM under 2 T magnetic field. The saturation magnetizations decrease with the increasing the cathode potential. The parallel and perpendicular hysteresis curves were measured and the easy axis of the multilayers is found in the parallel configuration. The magnetoresistance measurements were determined by the VDP method under 1.2 T magnetic field. The highest GMR value is found to be 16.50 % in the multilayer produced at −1.8 V cathode potential, and this multilayer exhibits the highest GMR sensitivity. Consequently, the Co and Fe amount easily deposit at high cathode potential for the magnetic layers but, high saturation magnetization and the GMR are obtained at −1.8 V. However, the better surface morphology and the GMR sensitivity are found in the multilayer produced at −2.8 V cathode potential.

Acknowledgements

This paper was financially supported by Balikesir University under Grant No. BAP 2012/33. The authors would like to thank to Uludag University BAP under Grant No. UAP(F)-2010/56 for the electrodeposition system. The authors are grateful to Dr. H. Guler for XRD measurement, Balikesir University, Turkey and thanks to UNAM at Bilkent University, Turkey for SEM and EDX measurements. The authors thank to State Planning Organization, Turkey under Grant No. 2005K120170 for VSM system and Balikesir University BAP under Grant No. 2001/02 and 2005/18 for MR system.

References

[1] R. L. White, IEEE Trans. Magn. **30**(2), 346 (1994).
[2] H. van den Berg, U. Hartmann, R. Coehoorn, M. Gijs, P. Grünberg, T. Rasing, K. Röll, Magnetic Multilayers and Giant Magnetoresistance: Fundamentals and Industrial Applications. Springer Series in Surface Sciences. Springer Berlin Heidelberg 2013.
[3] C. Reig, S. Cardoso, S. Mukhopadhyay, Giant Magnetoresistance (GMR) Sensors: From Basis to State-of-the-Art Applications. Smart Sensors, Measurement and Instrumentation. Springer Berlin Heidelberg 2013.
[4] J. M. Daughton, J. Magn. Magn. Mater. **192**(2), 334 (1999).
[5] P. P. Freitas, R. Ferreira, S. Cardoso, F. Cardoso, J. Phys. Condens. Matter. **19**(16), 165221 (2007).
[6] G. Rizzi, J. R. Lee, P. Guldberg, M. Dufva, S. X. Wang, M. F. Hansen, Biosens. Bioelectron. **93**, 155 (2017).
[7] P. Grünberg, R. Schreiber, Y. Pang, M. B. Brodsky, H. Sowers, Phys. Rev. Lett. **57**(19), 2442 (1986).
[8] M. N. Baibich, J. M. Broto, A. Fert, F. N. Vandau, F. Petroff, P. Eitenne, G. Creuzet, A. Friederich, J. Chazelas, Phys. Rev. Lett. **61**(21), 2472 (1988).
[9] M. Alper, K. Attenborough, R. Hart, S. J. Lane, D. S. Lashmore, C. Younes, W. Schwarzacher, Appl. Phys. Lett. **63**(15), 2144 (1993).
[10] S. S. P. Parkin, Z. G. Li, D. J. Smith, Appl. Phys. Lett. **58**(23), 2710 (1991).
[11] D. H. Mosca, F. Petroff, A. Fert, P. A. Schroeder, W. P. Pratt, R. Laloee, J. Magn. Magn. Mater. **94**(1-2), L1 (1991).
[12] G. R. Harp, S. S. P. Parkin, R. F. C. Farrow, R. F. Marks, M. F. Toney, Q. H. Lam, T. A. Rabedeau, A. Cebollada, R. J. Savoy, Mater. Res. Soc. Symp. P. **313**, 41 (1993).
[13] H. El Fanity, K. Rahmouni, M. Bouanani, A. Dinia, G. Shmerber, C. Meny, P. Panissod, A. Cziraki, F. Cherkaoui, A. Berrada, Thin Solid Films **318**(1-2), 227 (1998).
[14] I. Bakonyi, L. Peter, Z. E. Horvath, J. Padar, L. Pogany, G. Molnar, J. Electrochem. Soc. **155**(11), D688 (2008).
[15] M. Haciismailoglu, M. Alper, H. Kockar, Sensor Lett. **11**(1), 106 (2013).
[16] N. Rajasekaran, J. Mani, B. G. Toth, G. Molnar, S. Mohan, L. Peter, I. Bakonyi, J. Electrochem. Soc. **162**(6), D204 (2015).
[17] D. Reyes, N. Biziere, B. Warot-Fonrose, T. Wade, C. Gatel, Nano Lett. **16**(2), 1230 (2016).
[18] M. R. Parker, S. Hossain, D. Seale, J. A. Barnard, M. Tan, H. Fujiwara, IEEE T. Magn. **30**(2), 358 (1994).
[19] Q. Huang, C. Bonhote, J. Lam, L. R. Romankiw, ECS Trans. **3**(25), 143 (2007).
[20] B. G. Toth, L. Peter, L. Pogany, A. Revesz, I. Bakonyi, J. Electrochem. Soc. **161**(4), D154 (2014).
[21] T. Sahin, H. Kockar, M. Alper, J. Magn. Magn. Mater. **373**(0), 128 (2015).
[22] A. Tekgul, M. Alper, H. Kockar, J. Magn. Magn. Mater. **421**, 472 (2017).
[23] D. M. Edwards, J. Mathon, R. B. Muniz, S. S. P. Parkin, J. Magn. Magn. Mater. **114**(3), 252 (1992).
[24] K. D. Bird, M. Schlesinger, J. Electrochem. Soc. **142**(4), L65 (1995).
[25] M. A. M. Gijs, M. T. Johnson, A. Reinders, P. E. Huisman, R. J. M. Vandeveerdonk, S. K. J.

Lenczowski, R. M. J. Vangansewinkel, Appl. Phys. Lett. **66**(14), 1839 (1995).
[26] Y. Ueda, N. Hataya, H. Zaman, J. Magn. Magn. Mater. **156**(1-3), 350 (1996).
[27] Y. Hayashi, C. G. Lee, B. H. Koo, T. Sato, M. Arita, M. Masuda, Phys. Status Solidi A. **201**(8), 1658 (2004).
[28] B. G. Toth, L. Peter, I. Bakonyi, J. Electrochem. Soc. **158**(11), D671 (2011).
[29] A. Tekgul, M. Alper, H. Kockar, H. Kuru, J. Mater. Sci. **52**(6), 3368 (2017).
[30] A. Tekgul, H. Kockar, H. Kuru, M. Alper, Z. Naturforsch. A. **73**(2), 127 (2018).
[31] A. Tekgul, H. Kockar, H. Kuru, M. Alper, C. G. Unlu, J. Electron. Mater. **47**(3), 1896 (2018).
[32] C. Bran, E. M. Palmero, Z.-A. Li, R. P. del Real, M. Spasova, M. Farle, M. Vázquez, J. Phys. D Appl. Phys. **48**(14), 145304 (2015).
[33] M. Tsunoda, H. Arai, D. Takahashi, S. Miura, M. Takahashi, J. Magn. Magn. Mater. **240**(1-3), 189 (2002).
[34] Y. Saito, K. Inomata, Jpn. J. Appl. Phys. **30**(10A), L1733 (1991).
[35] E. M. Kakuno, R. C. da Silva, N. Mattoso, W. H. Schreiner, D. H. Mosca, S. R. Teixeira, J. Phys. D Appl. Phys. **32**(11), 1209 (1999).
[36] A. Tekgul, M. Alper, H. Kockar, M. Safak, O. Karaagac, J. Nanosci. Nanotechno. **10**(11), 7783 (2010).
[37] A. Ramazani, M. Ghaffari, M. A. Kashi, F. Kheiry, F. Eghbal, J. Phys. D Appl. Phys. **47**(35), 355003 (2014).
[38] A. Tekgul, M. Alper, H. Kockar, M. Haciismailoglu, J. Mater. Sci. Mater. Electron. **26**(4), 2411 (2015).
[39] A. Tekgül, M. Alper, H. Kockar, J. Mater. Sci. Mater. Electron. **27**(10), 10059 (2016).
[40] A. Tekgul, H. Kockar, M. Alper, J. Supercond. Nov. Magn. **31**(7), 2195 (2018).
[41] A. Tekgül, H. Köçkar, M. Alper, Thin Solid Films. **673**, 7 (2019).
[42] I. Bakonyi, L. Peter, Prog. Mater. Sci. **55**(3), 107 (2010).
[43] H. Kuru, H. Kockar, M. Alper, J. Magn. Magn. Mater. **373**, 135 (2015).
[44] A. Karpuz, H. Köçkar, M. Alper, O. Karaagac, M. Haciismailoglu, Appl. Surf. Sci. **258**, 4005 (2012).
[45] H. Hu, M. Tan, L. Liu, J. Alloys Compd. **715**, 384 (2017).
[46] A. Karpuz, H. Köçkar, S. Çölmekçi, M. Uçkun, J. Supercond. Nov. Magn. **33**, 463 (2020).
[47] W. Wright, Powder Metallurgy **2**(4), 79 (1959).
[48] T. C. Schulthess, W. H. Butler, Phys. Rev. Lett. **81**(20), 4516 (1998).

*Corresponding author: atakantekgul@gmail.com